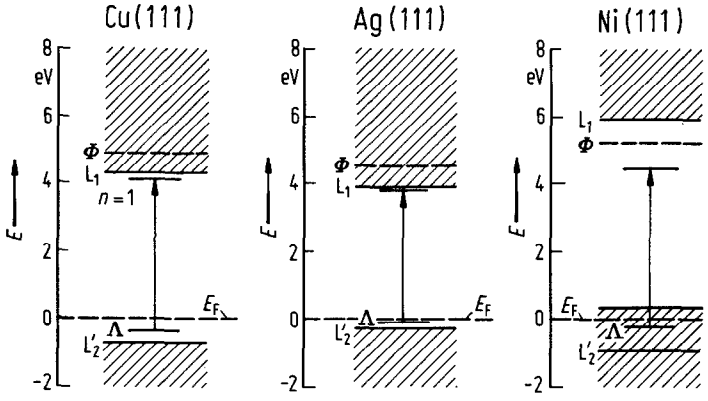

Fig. 28. Cu, Ag, Ni. Energy level diagram for $k_{\parallel}=0$ for the (111) surfaces studied by two photon photo-emission. Hatched areas indicate bulk band continua [89S2].

3.1.2.4 Work function data

(Tables 14 ··· 20, Figs. 29 ··· 31)

The work function Φ can be defined as the minimum energy required to extract one electron from the metal. If this definition is formulated more precisely, the following expression can be deduced [70L1, 79H10]:

$$\Phi = \Delta\phi - \bar{\mu}, \tag{3}$$

where $\Delta\phi$ depends on the surface and the chemical potential $\bar{\mu}$ depends on bulk properties only. Under these conditions the electron is thought to be at a distance larger than 10^3 nm above the surface and at zero kinetic energy. This distance is large enough so that the image potential is negligible, but small enough so that the potential is determined by the surface only and is not distorted by fields from the edges of the finite crystal [79H10].

The split of Φ into two parts in Eq. (3) is also plausible from qualitative arguments. Besides the bulk component ($-\bar{\mu}$) there is a surface contribution due to the spill-out of the electrons at the surface into the vacuum which leaves behind a positively charged region. This dipole layer at the surface increases the work function. This consideration also makes it plausible that Φ depends on the surface atomic density, i.e. on the crystallographic orientation. The general trend is that $\Delta\phi$ increases with the surface atomic density.

Theory

We want to make only some brief remarks on the theory of the work function. There is a number of excellent reviews and contributions to which the reader is referred [79H10, 81K4, 84W2, 91L1, 92M1]. Φ is certainly a basic property of any surface. The accuracy of its calculation benefits from any progress in electronic structure calculations of surfaces. On the other hand, it is obvious that Φ is strongly correlated also with the atom density at the surface, i.e. also with any known or anticipated reconstruction or relaxation of the surface. Since there are still many open questions in this field, a similar number of questions is open in the field of work function calculations.

Of great importance for the – at least qualitative – discussion of the orientational dependence of Φ was the work of Smoluchowski [41S1]. He showed that a lateral smoothing of the electron density leads to a lowering of the total energy. The electron density contour is smoother than the background boundary. This "Smoluchowski smoothing" leads generally to a reduction of Φ especially for the more open surfaces. Finnis and Heine [74F2] showed that the same effect leads to an inwards relaxation of the top layer.

There is general agreement, e.g. [79H10, 82I1, 91L1], that the first break-through in calculating Φ was achieved by Lang and Kohn using density-functional formalism and the jellium model [70L1, 71L1, 73L1]. Fig. 29 and Table 14 exhibit quite a good agreement between their jellium calculations and the experimental value for a number of sp metals for the whole range of Wigner-Seitz radii between 2 and 6 atomic units.

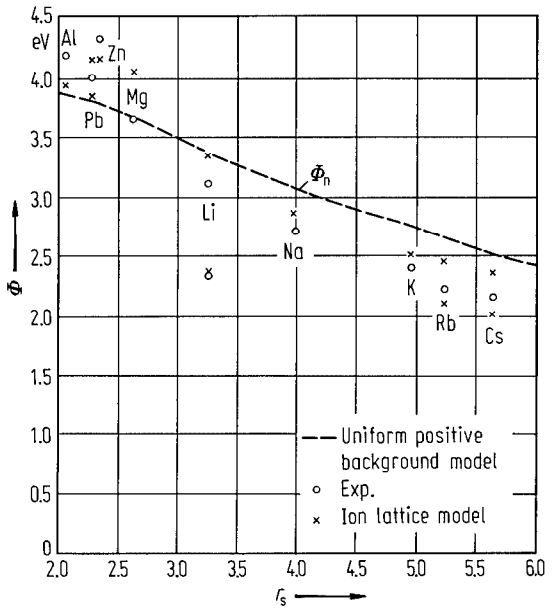

Fig. 29. Comparison of theoretical values of the work function with the results of experiments on polycrystalline samples. Φ_n is the work function in the uniform-background model. The Φ values in the ion-lattice model were computed for the (110), (100), and (111) faces of the cubic metals and the (0001) face of the hcp metals (Zn and Mg). For qualitative purposes, the simple arithmetic average of these values for each metal is indicated by a cross (two crosses are shown for the cases in which there were two possible pseudopotential radii). The experimental and theoretical points for Zn should be at $r_s = 2.30$; they have been shifted slightly on the graph to avoid confusion with the data for Pb [71L1].

Table 14. Theoretical and experimental work functions of nine simple metals. Φ_u is the work function for the uniform-background model; $\delta\Phi$ is the first-order pseudopotential correction; $\Phi = \Phi_u + \delta\Phi$ (rounded to the nearest 0.05 eV); r_c is the pseudopotential core radius. Experimental values Φ_{exp} for polycrystalline samples were taken from Table 19. The most densely packed faces for the various structures are: fcc (111), hcp (0001), bcc (110) [71L1].

Metal	Structure	r_s	Φ_u [eV]	r_c	$\delta\Phi$ [eV]			Φ [eV]			Φ_{exp} [eV]
					(110)	(100)	(111)	(110)	(100)	(111)	(polycrystalline)
Al	fcc	2.07	3.87	1.12	− 0.21	0.32	0.19	3.65	4.20	4.05	4.3
Pb	fcc	2.30	3.80	1.47	0	0.72	0.33	3.80	4.50	4.15	4.2
Zn	hcp	2.30	3.80	1.27	0.36[1])			4.15[1])			4.2
Mg	hcp	2.65	3.66	1.39	0.38[1])			4.05[1])			3.7
Li	bcc	3.28	3.37	1.06	0.19	− 0.05	− 0.13	3.55	3.30	3.25	2.9
Na	bcc	3.99	3.06	1.67	0.03	− 0.29	− 0.39	3.10	2.75	2.65	2.4
K	bcc	4.96	2.74	2.14	0.01	− 0.34	− 0.40	2.75	2.40	2.35	2.3
Rb	bcc	5.23	2.63	2.13	0.03	− 0.26	− 0.34	2.65	2.35	2.30	2.2
Cs	bcc	5.63	2.49	2.16	0.10	− 0.21	− 0.27	2.60	2.30	2.20	2.1

[1]) For (0001) face.

The change in self-consistent field (ΔSCF) expression is a generalization of the one given by Lang and Kohn. Monnier and Perdew [78M4] showed that the ΔSCF expression is much less profile-sensitive than other exact expressions for the work function and is therefore well suited for use with approximate profiles. The "variational self-consistent" profiles (more realistic than jellium profiles) are applied to evaluate the ΔSCF work function for a few selected surfaces of simple metals, among them the three low-index faces of Al, for which agreement with experiment is found to be good (see Table 15) [78M4].

Table 15. Experimental and theoretical work functions for the three low index planes of Al [78M4].

	Φ [eV]		
	Al(111)	Al(100)	Al(110)
Experiment:			
[76G3]	4.24 (2)	4.41 (3)	4.28 (2)
[73E1]	4.26 (2)	4.20 (3)	4.06 (3)
Theory:			
[78M4]	4.27	4.25	4.02
[71L1]	4.05	4.20	3.65
[73C1]	–	4.49	4.83[1])
[76T1]	4.26	–	–
[75C1]	5.27	–	–

[1]) Includes relaxation of first lattice plane.

Table 16. Work functions for a few selected metals and faces, calculated from the ΔSCF expression by Lang and Kohn [71L1] using the perturbational self-consistent profiles and calculated here using the variational self-consistent profiles [78M4].

		Φ [eV]	
Metal	face	[71L1]	[78M4]
Pb	(111)	3.85	–
	(100)	3.95	4.10
	(110)	3.80	3.90
Zn	(0001)	4.15	4.30
Mg	(0001)	4.05	4.18
Na	(110)	3.10	3.13
	(100)	2.75	2.84
	(111)	2.65	2.76

Bohnen and Ying [80B1] calculated the work function for the alkali metals by a direct determination of the density matrix in a local orbital basis (see Table 17). The method is based on a variational treatment of the ground state energy applying the Hohenberg-Kohn-Sham functional formalism.

Table 17. Face-dependent work function for Na, K, Rb, and Cs [80B1].

Metal	face	Φ [eV] Density-matrix method	Jellium [1]	[2]	Experiment[3] (polycrystalline)
Na	(100)	2.7	2.75	2.84	2.4
	(110)	3.1	3.1	3.13	
K	(100)	2.8	2.4	2.7	2.3
	(110)	3.2	2.75	2.9	
Rb	(100)	2.3	2.1	2.6	2.2
	(110)	2.6	2.2	2.9	
Cs	(100)	2.3	1.9	2.3	2.1
	(110)	2.5	2.25	2.8	

[1] [70L1, 71L1]
[2] [78M3, 78M4]
[3] From Table 19.

The next important step is to include the d electrons in order to calculate the work function of the transition metals. So far, there are no systematic calculations throughout the periodic table which agree with the experimental data. This does not exclude very good results for some special cases which are collected in Table 20. There are several facts which make the inclusion of d electrons difficult. First, the d electrons are more localized than the sp electrons. Second, there is some redistribution between s and d electrons during formation of the solid state, and, third, this redistribution can be different at the surface [84W2].

It is well recognized that many physical properties including Φ exhibit a parabola-like dependence when going through a series of transition metals. This observation can be qualitatively explained by the sequence of first filling the bonding and then the antibonding orbitals of the d states. Since many physical properties are influenced by the filling sequence, its influence on Φ is not clear a priori. So it can be argued that the d orbitals exert an inward force on the surface against the pressure of the sp electrons with their tendency to spill out into the vacuum. Quite obviously, this may influence surface relaxation as well as Φ.

In order to visualize the complexity of this question, we mention the work of Weinert and Watson [84W2]. In an otherwise unrealistic model, since it gives no face dependence, i.e. a constant dipole contribution, they used the so-called Mattheis-construct [64M1]. Results of this calculation are shown in Table 18 and Fig. 30.

The solid line in Fig. 30 is the $\bar{\mu}'$ of Table 18 where the chemical potential is measured with respect to the crystal zero and a constant valence charge density is assumed in the muffin-tin region. The upper bound of the shaded region is associated with placing all the charge of the interstitial region on the surface of the muffin-tin sphere while the lower bound has the charge at the Wigner-Seitz radius. The $\bar{\mu}'$ for the 3d and 4d rows peak at Cr and Mo, respectively. Following Weinert and Watson [84W2], this is readily understood since these metals have half-filled d bands where the "bonding" levels are occupied and the "antibonding" levels are not. Maximum cohesion is obtained by compressing the atoms so as to gain the bonding energy associated with having a large bandwidth. This is done at the cost of raising the band center of gravity so that $\bar{\mu}'$ lies shallower than it does in the metals of the neighboring elements.

Finally, we mention a most recent result from a density functional theory calculation of surface energies, surface relaxations and work functions for a number of low-index surfaces of the 4d transition metals from Y to Ag [92M1]. Fig. 31 exhibits the result of the work function calculation. The basic rising trend across the series follows closely that of the first ionization potential of the free atoms. From Pd to Ag, part of the extra electron goes into the sp band above the full d band, increasing the Fermi energy and reducing the work function [92M1]. It is interesting to note that the calculated trends of the top-layer relaxation can be understood as an interplay between sp smoothing and localization of d bands [92M1].

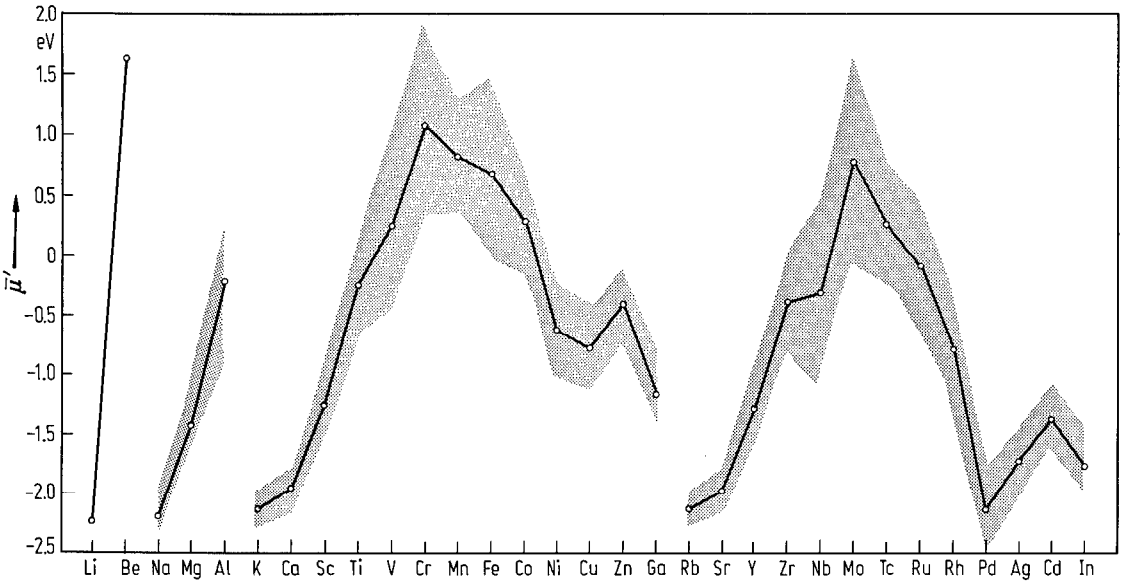

Fig. 30. Chemical potentials relative to the "crystal zero". The upper bound of the shaded region is associated with placing all the charge of the interstitial region on the surface of the muffin-tin sphere while the lower bound has the charge at the Wigner-Seitz radius [84W2].

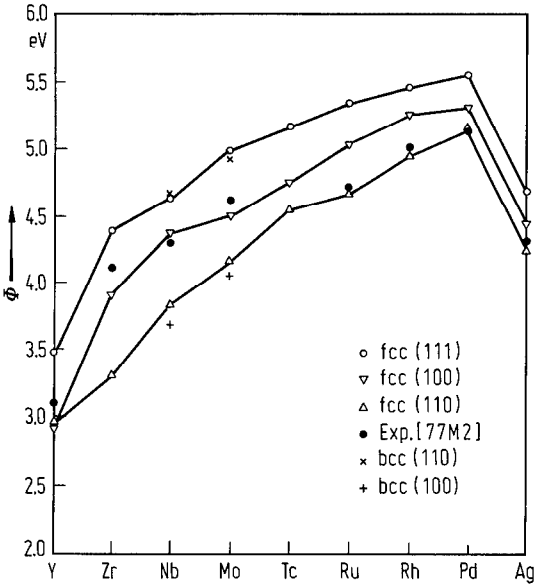

Fig. 31. Calculated surface-resolved work function Φ as compared to the experimental polycrystalline values [92M1].

Table 18. Calculated values of the work-function contributions. The chemical potentials $\bar{\mu}$, $\bar{\mu}'$ are given with respect to the average electrostatic potential and the "crystal zero", respectively. The calculated work functions Φ and corresponding dipole barriers D' relative to the "crystal zero" are obtained from free-atomic densities (Φ_0, D'_0) and for atoms in a well ($\tilde{\Phi}$, $\tilde{D}'$). These are compared with the D' deduced from experimental values of the work function Φ_{exp} [84W2].

Element	$\bar{\mu}$ [eV]	$\bar{\mu}'$ [eV]	Φ_0 [eV]	D'_0 [eV]	$\tilde{\Phi}$ [eV]	$\tilde{D}'$	Φ_{exp}[1]) [eV]	D' [eV]
H	3.7	− 0.2	7.2	7.0	4.0	3.8		
Li	0.8	− 2.2	7.5	5.3	4.3	2.1	2.9	0.7
Be	9.1	1.6	9.2	10.8	4.8	6.4	5.0	6.6
Na	1.8	− 2.2	4.8	2.6	3.1	0.9	2.8	0.6
Mg	5.5	− 1.4	5.3	3.9	3.5	2.1	3.7	2.3
Al	9.7	− 0.2	7.5	7.3	4.2	4.0	4.3	4.1
K	2.5	− 2.1	4.0	1.9	2.8	0.7	2.3	0.2
Ca	6.0	− 2.0	5.9	3.9	4.0	2.0	2.9	0.9
Sc	10.1	− 1.3	7.6	6.3	3.9	2.6	3.5	2.2
Ti	14.4	− 0.3	8.9	8.6	4.4	4.1	4.3	4.0
V	17.8	0.2	10.0	10.2	5.1	5.3	4.3	4.5
Cr	20.3	1.1	9.7	10.8	4.8	5.9	4.5	5.6
Mn	20.7	0.8	9.7	10.5	5.1	5.9	4.1	4.9
Fe	20.8	0.7	8.9	9.6	4.8	5.5	4.5	5.2
Co	20.3	0.3	8.7	9.0	5.0	5.3	5.0	5.3
Ni	18.4	− 0.6	8.1	7.5	5.1	4.5	5.2	4.6
Cu	16.6	− 0.8	6.6	5.8	4.2	3.4	4.7	4.1
Zn	14.9	− 0.4	4.9	4.5	3.2	2.8	4.3	3.9
Ga	12.4	− 1.1	6.6	5.5	4.1	3.0	4.2	3.1
Rb	3.1	− 2.1	3.6	1.5	2.7	0.6	2.2	0.1
Sr	7.0	− 2.0	5.4	3.0	3.7	1.7	2.6	0.6
Y	12.1	− 1.3	7.0	5.7	3.8	2.5	3.1	1.8
Zr	16.9	− 0.4	7.9	7.5	4.3	3.9	4.1	3.7
Nb	20.0	− 0.3	8.7	8.4	5.0	4.7	4.3	4.0
Mo	23.8	0.8	8.4	9.2	4.6	5.4	4.6	5.4
Tc	24.2	0.2	8.7	8.9	5.2	5.4		
Ru	24.5	− 0.1	8.3	8.2	5.1	4.9	4.7	4.6
Rh	23.2	− 0.8	8.0	7.2	5.3	4.5	5.0	4.2
Pd	20.2	− 2.1	7.9	5.8	5.7	3.6	5.1	3.0
Ag	17.9	− 1.7	5.7	4.0	4.1	2.4	4.3	2.6
Cd	15.3	− 1.4	4.6	3.2	3.4	2.0	4.2	2.8
In	13.2	− 1.8	5.7	3.9	4.0	1.2	4.1	1.3

[1]) ≙ [77M2]

Measurements

The latest collections of work function data are more than 10 years old. Here we like to mention the widely used collection of Michaelson [77M2] and the comprehensive review of Hölzl and Schulte [79H10] which includes also the work function change due to adsorbates. Both collections are based largely on photoelectric work function measurements, among them the extensive investigation of Eastman [70E1] on evaporated metal films. In this method the quantum yield $Y(\omega)$ versus photon energy $h\nu$ above threshold is measured and Φ is evaluated from the so-called Fowler plot:

$$[Y(\omega)]^{1/2} \alpha(h\nu - \Phi). \tag{4}$$

During the last 15 years, a further absolute method for Φ determination has been developed. This method is based on ARUPS and the use of laboratory resonance lamps. The advantage in using these lamps is that $h\nu$ is known very accurately. The energy for the He Iα line, e.g., is $h\nu = 21.217$ eV [70T1].

If one collects all electrons without cutting off some at the low energy end of the spectrum, one measures the width W of the photoelectron energy distribution curve. For a metal this is quite easy, since both the secondary electron threshold as well as the Fermi edge exhibit a large enough intensity. Thus, the work function can be determined from

$$\Phi = h\nu - W. \tag{5}$$

By this method absolute work function values can be determined with an accuracy of ± 10 meV under the following conditions:

(1) The measurements have to be performed in an angle-resolved mode. Angle-integrated modes collect, with increasing kinetic energy, an increasing number of secondary electrons with $k_{\parallel} \neq 0$. The threshold can therefore have a width of up to 1 eV and is no sharp level. That is why an extrapolation procedure has to be used which always includes some degree or arbitrariness.

(2) The spectrometer sample configuration should be of such a geometry that a planar electric field is built in front of the sample, if one supplies the sample with a bias voltage of, e.g., -2 Volt. This voltage accelerates all photoelectrons by 2 eV and ensures that the full spectrum, including the electrons of the true secondary-electron threshold, enters the spectrometer. Both conditions are fulfilled for the ARUP spectrometer (ADES 400, VG Scientific) we use in our laboratory. For a Pt(111) surface and a pass energy of the spectrometer of 5 eV we have measured a linear increase of intensity from 10 ··· 90% within 120 meV at the secondary-electron threshold and a 10 ··· 90% drop of intensity within 140 meV at the Fermi edge. Under these conditions the secondary-electron threshold is as sharp as the Fermi edge. We have therefore included the energy resolution of our spectrometer at both edges.

Going beyond the old data collections we have included Φ values from ARUPS measurements. For comparison we have also listed the former values of Michaelson [77M2]. The values of Michaelson are identical to those given by Hölzl and Schulte [79H10]. The difference between these two collections is that Michaelson makes some judgement and gives the "best values", whereas Hölzl and Schulte collect all values which have been measured under reasonably clean conditions. We follow Michaelson and try to give best values. We have rounded the values for polycrystalline samples to 0.1 eV.

Table 19. Work function for clean metals. For single-crystal surfaces the surface is indicated in round brackets, polycrystalline metal films are not indicated. The experimental method is indicated as follows: P: photoelectric; A: angle-resolved photoelectron spectroscopy; C: contact-potential difference; T: thermionic; F: field emission; D: diode (retarding field) method.

Element	Φ [eV]	Method	Ref.	Remark
Ag	4.3	P	75D3	
	4.22(100)	P	82C1	[1]
	4.14(100)	P	82C1	[1]
	4.46(111)	P	82C1	[1]
	4.45(111)	A	91H1	
	4.56(111)	A	87G4, 86G3	
	4.42(100)	A	87G4	
	4.35(100)	A	87R1	
Al	4.3	P	73E1	
	4.20(100)	P	73E1	
	4.06(110)	P	73E1	
	4.26(111)	P	73E1	
	4.41(100)	P	76G3	
	4.28(110)	P	76G3	
	4.24(111)	P	76G3	
	4.20(111)	A	88F2	
Au	5.1	P	70E1	
	5.22(100)	A	78H2	
	5.20(110)	A	78H2	
	5.26(111)	A	78H2	
Ba	2.50	A	87J2	
Be	5.0	P	74G1	
Bi	4.2	P	62S1	
Ca	2.9	P	71G1, 71K1	
Cd	4.2	C	55A1	
Ce	2.9	P	70E1	
Co	5.0	P	70E1	
	5.2(0001)	A	91H3	
Cr	4.5	P	70E1	
Cs	2.30	A	92S1	
Cu	4.65	P	70E1	
	4.59(100)	P	72G2	
	4.48(110)	P	72G2	

[1]) Values [75D3] in the listing of [77M2] have been revised later in [82C1].

Table 19 (continued)

Element	Φ [eV]	Method	Ref.	Remark
	4.85(111)	P	75G1	
	4.53(112)	P	72G2	
	4.63(100)	A	87G4	
	4.5(110)	A	82M1	
	4.88(111)	A	86G3, 88K1	
Eu	2.5	P	70E1	
Fe	4.5	P	70E1	
	4.67(100)	P	72U1	
	4.81(111)	P	69K1	
	5.05(110)	A	80P3	
Ga	4.3	P	74K1	at 200 °C
Gd	3.1	P	70E1	
Hf	3.9	P	70E1	
Hg	4.5	P	67L1	
In	4.1	P	71P1	
Ir	5.3	T	66W1	
	5.42(110)	F	73S1	
	5.76(111)	F	73S1	
	5.67(100)	F	74N1	
	5.00(210)	F	74N1	
K	2.3	P	72V1	
La	3.5	P	70E1	
Li	2.9	F	68O1	
Lu	3.3	C	71B2	
Mg	3.7	P	64G1	
Mn	4.1	P	70E1	
Mo	4.6	P	70E1	
	4.53(100)	P	74B1	
	4.95(110)	P	74B1	
	4.55(111)	P	74B1	
	4.36(112)	P	74B1	
	4.50(114)	P	74B1	
	4.55(332)	P	74B1	
Na	2.4	P	72V1	
	2.9(110)	D	77A1	

Table 19 (continued)

Element	Φ [eV]	Method	Ref.	Remark
Nb	4.3	P	70E1	
	4.02(001)	T	74L1	
	4.87(110)	T	74L1	
	4.36(111)	T	74L1	
	4.63(112)	T	74L1	
	4.29(113)	T	74L1	
	3.95(116)	T	74L1	
	4.18(310)	T	74L1	
Nd	3.2	P	70E1	
Ni	5.15	P	70E1	
	4.89(100)	T	68K1	[2]
	4.64(110)	T	68K1	
	5.22(111)	T	68K1	
	4.55(110)	A	82J3	
	5.25(111)	A	86G3	
	4.95(100)	D	75P1	[3]
Os	4.8	T	66W1	
Pb	4.2(1 ML)	A	83G2	
	4.05(111)	A	88J5	
Pd	5.1	P	74N1	
	5.60(111)	A	90B5	
	5.55(111)	A	87K3	
Pt	5.65	P	66W1	
	5.93(111)	F	73N1	[4]
	5.84(100)	F	73N1	[4]
	5.12(331)	F	73N1	[4]
	5.20(320)	F	73N1	[4]
	5.84(100)	P	90R5	
	5.82(111)	A	92J1	
Rb	2.2	P	67L1	
Re	5.0	T	66W1	
	5.75(1011)	F	68O1	
Rh	5.0	P	74N1	
Ru	4.7	P	74N1	
	5.4	A	85W4	
	5.37(0001)	A	92S2	
	5.1($10\bar{1}0$)	A	92G1	

[2]) Fowler plot is taken (in the temperature range of 1250–1579 K).
[3]) Comparison with Cu(100) and assuming Φ(Cu(100)) = 4.59 eV.
[4]) Assuming a mean value of Φ = 5.32 eV for the whole tip.

Table 19 (continued)

Element	Φ [eV]	Method	Ref.	Remark
Sb	4.55(amorph.)		72G3	
	4.7(100)		71G2	
Sc	3.5	P	70E1	
Sm	2.7	P	70E1	
Sn	4.4	C	63S1	
Sr	2.6	T	69A1	
Ta	4.25	T	66W1	
	4.15(100)	T	66P1	
	4.80(110)	T	66P1	
	4.00(111)	T	66P1	
Tb	3.0	P	69N1	
Th	3.4	T	66E1	
Ti	4.3	P	70E1	
	4.58(0001)	F	81J1	
Tl	3.8	C	38K1	
U	3.6	P, C	67H1	
	3.73(100)	P, C	68L1	
	3.90(110)	P, C	68L1	
	3.67(113)	P, C	68L1	
V	4.3	P	70E1	
W	4.6	C	63H1	[5]
	4.63(100)	F	73S1	
	5.25(110)	F	73S1	
	4.47(111)	F	73S1	
Y	3.1	P	70E1	
Zn	4.3	P	62S1	
	4.9(0001)	C	72B1	
Zr	4.05	P	70E1	

[5]) For high-index surfaces see [79H10].

Table 20. Theoretical values of work function. Further theoretical values are listed in Figs. 29 and 31 and Tables 13 ··· 17. The crystal face is noted in round brackets.

Element	Φ [eV]	Ref.
Ag	4.2(100)	80S1
Al	4.27(111)	80M1
	4.73(111)	81W1
Ba	2.6(100)	90C2
Cu	4.5(100)	79G1
Hf	4.2(100)	90C2
In	4.6(100)	90C2
K	2.39(100)	79B3
Li	3.58 (hcp, 2 layers)	90B2
Na	3.1(110)	89R1
Ni	5.1(100)	80A1
Pb	4.4(100)	90C2
Pd	5.8(111)	78L1
	5.0(100)	81G1
Rh	5.1(111)	82F1
	5.6(111)	83F2
	5.5(100)	83F2
	4.8(100)	82G1
Ru	5.4(0001)	82F1
Sr	2.8(100)	90C2
Ta	4.3(100)	84K2
Ti	3.8(0001)	79F2
W	4.5(100)	80P2